Optical bistability involving photonic crystal microcavities and Fano line shapes

A. R. Cowan and Jeff F. Young

Department of Physics and Astronomy, University of British Columbia, Vancouver, BC, Canada V6T 1Z4
(Received 21 May 2003; published 20 October 2003)

The reflectivity of a single-channel waveguide mode upon resonantly coupling to a Kerr-active nonlinear resonant cavity is calculated analytically, including the effects of two-photon absorption. The resonant reflectivity takes the form of a Fano resonance because the solution includes linear reflections from perturbations downstream of the localized cavity. Instead of using a Hamiltonian formulation of the scattering problem, an intuitive set of basis states is used to expand the Green's function of the electric field wave equation. All resulting overlap functions describing the linear coupling between guided and localized states, and the nonlinear renormalization of the material's refractive index, are in terms of well-defined physical quantities. Although derived in the context of photonic crystal-based waveguides and cavities, the treatment is valid for any low-loss waveguide-resonator geometry that satisfies specific weak coupling criteria. For a cavity consisting of $Al_{0.18}Ga_{0.82}As$, hosting a localized mode at 1.55 μm with a Q of 4000 and a mode volume of 0.055 μm^3, we predict the onset of bistable reflection at incident powers of ~ 40 mW. The downstream reflections lead to hysteresis loops in the reflectivity that are topologically distinct from conventional Lorentzian-derived loops characteristic of isolated Fabry-Perot cavities. We provide a stability argument that reveals the unstable branches of these unique hysteresis loops, and we illustrate some of the rich bistable behaviors that can be engineered with such downstream sources.

PACS number(s): 42.70.Qs, 42.65.Pc

I. INTRODUCTION

Ideal photonic crystals offer the intriguing possibility of artificially confining and routing photons in three dimensions (3D) without radiation losses [1,2]. This is accomplished by introducing "defects" into an otherwise perfectly periodic photonic crystal (PC), such that localized modes are created with energies that lie within the crystal's photonic band gap. These modes can be confined on length scales comparable to the relevant photon wavelength, in 2D for line defects and in 3D for fully localized microcavities. Such tight confinement offers the potential for fabricating ultrasmall, optical "integrated circuits" in which light is piped through lossless waveguides and filtered through the engineered coupling of these waveguides with fully localized microcavities. Yariv and co-workers have studied such waveguide-resonator coupling in a variety of geometries [3]. Add-drop filters based on coupled waveguides and cavities have been proposed [4–7]. Resonant tunneling of the guided mode through a localized cavity mode has been both theoretically studied [3] and experimentally observed in a slab waveguide based photonic crystal [8]. The vertical emission of guided light via a cavity in such planar photonic crystals has been demonstrated by Noda *et al.* [9].

The rich dispersion of *propagating* modes in bulk photonic crystals also offers new opportunities for engineering light propagation. Strongly dispersive parts of the band structure might be exploited for optical delay lines [10], dispersion compensation [11], or superprisms [12]. Engineerable dispersion is particularly interesting in the context of *nonlinear* optical processes. The periodic nature of these crystals can be exploited to achieve quasi-phase-matching, and the low group velocity of strongly dispersive photonic bands has been shown theoretically to increase nonlinear conversion efficiencies [13].

Several nonlinear studies of photonic crystals have been reported [14]. Most of this work has been theoretical, largely because it is still difficult to fabricate good quality 3D photonic crystals. However, there have been several nonlinear experimental studies of high-index-contrast 1D and 2D crystals that exhibit large pseudo-band-gaps [15–19]. One scheme for engineering harmonic conversion or optical bistability exploits strong local field effects in microcavities. Planar cavities can be formed between high-index-contrast 1D photonic crystal mirrors [17] or they can be accessed via leaky mode excitations of 2D planar photonic crystals [20,21]. In essence, these are all nonlinear Fabry-Perot-like cavities [22]. Taking the third-order Kerr effect (intensity dependent refractive index) as an example, it is well known that nonlinear 1D Fabry-Perot cavities exhibit optical bistability at incident power densities that scale as the inverse square of the cavity's quality factor $1/Q^2$. However, in many instances it is the total optical power and not the power density that is of paramount importance. The extent to which planar Fabry-Perot cavities can be used at low absolute powers is limited fundamentally by the in-plane dispersion of cavity modes. While this can be engineered to some extent in 2D planar photonic crystals [21], the ultimate means of reducing the absolute power levels required to observe optical bistability is to use a fully 3D localized photonic defect state as the nonlinear cavity and to access it by means of a single-mode 1D channel. One approach to achieve this goal involves coupling conventional 1D waveguides (fiber or ridge) to the high-order, high-Q whispering gallery modes of dielectric spheres [23]. The unique advantages offered by photonic crystals in this context are (i) that the localized mode volumes can be much smaller (less than a cubic wavelength) than those of high-order whispering gallery modes and (ii) that, in principle, the Q of the localized mode can be due entirely to its coupling with the 1D channel used to probe it,

rather than being limited by radiation losses. Of these two factors, the former is of much more practical relevance, since the Q values of high-order whispering gallery modes, though not infinite, are known to be much larger than can be achieved in any existing photonic crystal. A calculation involving photonic crystal-based cavities has predicted bistable switching at power levels as low as 2.6 mW (for $n_2 = 1.5 \times 10^{-17}$ m^2/W and a wavelength of 1.55 μm) [24].

This paper reports an analytic solution for the reflectivity of 1D PC waveguide modes incident on a nonlinear localized defect structure, allowing for arbitrary, but linear downstream reflections. The 1D and 0D defect structures are each assumed to support only single modes over the bandwidth of interest, and both the real (Kerr effect) and imaginary (two photon absorption) parts of the third-order susceptibility are included. Downstream, linear contributions to the background reflectivity are included because of the nontrivial effects they have on the nonlinear reflectivity of 2D planar photonic crystals when excited in the vicinity of leaky modes [21]. The formalism reported here treats both the linear and nonlinear parts of the scattering problem rigorously, not phenomenologically: analytic results are obtained by assuming the 1D waveguide modes are only weakly coupled to the single localized mode supported by the 0D defect structure (the high-Q limit). The Q value of the defect state and the linear and nonlinear coupling terms are all expressed explicitly in terms of matrix elements of the dielectric texture. Assuming realistic material parameters, it should be possible to observe bistable behavior in the waveguide reflectivity at optical power levels of ~ 40 mW, and the nature of the bistable loops can be controlled over a broad range by tailoring the downstream reflectivity. A simple stability argument that clearly describes the nature of these topologically distinct hysteresis loops is also presented.

The paper is organized as follows. In Sec. II we introduce the formalism by deriving expressions for the linear reflectivity and transmission of 1D waveguide modes interacting with a fully localized 0D defect cavity. Section II F generalizes this derivation to include a nonresonant, downstream scattering source. The nonlinear solution, including both real and imaginary components of the system's third-order susceptibility, is presented in Sec. III. Section IV contrasts the nature of bistable reflectivity for the cases of Lorentzian and Fano linear line shapes, and shows that bistable behavior should be achievable at power levels of the order of ~ 40 mW. We conclude in Sec. V.

II. COUPLED WAVEGUIDE AND CAVITY IN LINEAR REGIME

In this section we find the linear reflection and transmission of a 1D line defect waveguide mode in close spatial proximity to a 0D defect cavity. Our approach is based on a Green's function solution of Maxwell's equations expressed as a wave equation for the electric field vector. The Green's function is calculated by assuming it is given by a sum over a set of known basis states. While the derivation assumes the waveguide and cavity are designed in a photonic crystal it should be noted that the solution is valid for any waveguide-

resonator system that satisfies the weak coupling criterion and whose resonator exhibits low radiation losses (high Q). The formalism is therefore valid for appropriately designed planar photonic crystal circuits. In Sec. II A we define the equations to be solved. Section II B gives a detailed discussion of the approximations made in defining a set of basis states used to expand both the Green's function and the electric field that solves the wave equation. In Sec. II F we generalize the linear theory to include a downstream scattering source in addition to the resonant cavity. Section II E contains a discussion of how this derivation differs from related linear reflectivity calculations in the literature.

A. Waveguide-cavity system

Starting from the macroscopic Maxwell's equations it is straightforward to show that the electric field $\vec{E}(\vec{r}, \omega)$ satisfies the following wave equation:

$$\vec{\nabla} \times \vec{\nabla} \times \vec{E}(\vec{r}, \omega) = \tilde{\omega}^2 \vec{D}(\vec{r}, \omega) = \tilde{\omega}^2 \epsilon_t(\vec{r}) \vec{E}(\vec{r}, \omega), \quad (1)$$

where the fields are assumed to have a harmonic time dependence, $e^{i\omega t}$; $\tilde{\omega} = \omega/c$, where c is the speed of light in vacuum, and $\epsilon_t(\vec{r})$ is the dielectric constant distribution that includes the background photonic crystal, the 1D waveguide, and the localized cavity.

The transmission and reflection can be found by solving Eq. (1) for the electric field at the ends of the waveguide, $x \rightarrow \infty$ for transmission and $x \rightarrow -\infty$ for reflection, assuming that a waveguide mode was launched from one end ($x = -\infty$).

To facilitate a Green's function solution we write $\epsilon_t(\vec{r}) = \epsilon_w(\vec{r}) + 4\pi \chi^{0D}(\vec{r})$, where $\epsilon_w(\vec{r})$ is the dielectric constant of the photonic crystal including only the 1D line defect waveguide, and $\chi^{0D}(\vec{r}) = [\epsilon_t(\vec{r}) - \epsilon_w(\vec{r})]/4\pi$ describes the change in the dielectric constant that is needed to further introduce a 0D cavity. Equation (1) can then be written as

$$[\vec{\nabla} \times \vec{\nabla} \times - \tilde{\omega}^2 \epsilon_w(\vec{r})] \vec{E}(\vec{r}, \omega) = 4\pi \tilde{\omega}^2 \chi^{0D}(\vec{r}) \vec{E}(\vec{r}, \omega). \quad (2)$$

Note, in the above equation, and therefore for the rest of the derivation, we assume that the cavity is side coupled to the waveguide. However, with a minor redefinition of $\epsilon_w(\vec{r})$, the formulation can easily be modified to treat the case of a cavity embedded within the waveguide. Figure 1 is a schematic illustration of the waveguide-resonator geometry we consider.

In order to simplify the notation we revert to an operator formulation of Eq. (2)

$$(\mathcal{L} - \tilde{\omega}^2 \hat{\epsilon}_w) |\vec{\Psi}\rangle = 4\pi \tilde{\omega}^2 \hat{\chi}^{0D} |\vec{\Psi}\rangle, \quad (3)$$

where $\mathcal{L} = \vec{\nabla} \times \vec{\nabla} \times$ and the operators $\hat{\epsilon}_w$ and $\hat{\chi}^{0D}$ are defined as $\langle \vec{r} | \hat{\epsilon}_w | \vec{r}' \rangle = \epsilon_w(\vec{r}) \delta^{(3)}(\vec{r} - \vec{r}')$ and $\langle \vec{r} | \hat{\chi}^{0D} | \vec{r}' \rangle = \chi^{0D}(\vec{r}) \delta^{(3)}(\vec{r} - \vec{r}')$, respectively, where $\delta^{(3)}(\vec{r} - \vec{r}')$ is the three-dimensional Dirac delta function. The vector electric field is given by $\langle \vec{r} | \vec{\Psi} \rangle = \vec{E}(\vec{r}, \omega)$.
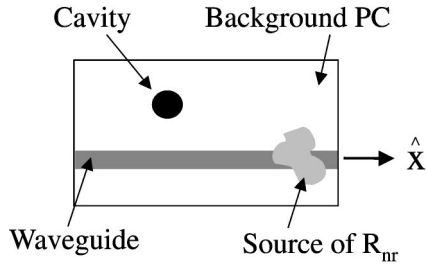
Cavity   Background PC

FIG. 1. Schematic diagram of the scattering geometry. A single-mode high-Q cavity is side coupled to a single-mode 1D waveguide that contains a downstream scattering center, which is the source of R_{nr} in Sec. II F.

Since $\mathcal{L}$ is a linear self-adjoint operator over real space, the homogeneous part of Eq. (3) defines the orthonormal set of eigenstates of a PC containing a 1D waveguide:

$$\mathcal{L}|\vec{\phi}_i\rangle = \widetilde{\omega}_i^2 \hat{\epsilon}_w |\vec{\phi}_i\rangle, \qquad (4)$$

where $\widetilde{\omega}_i$ are eigenvalues of the eigenstates $|\vec{\phi}_i\rangle$. These eigenstates can be calculated with a variety of techniques; one common approach is numerical finite difference time domain (FDTD) simulations. The completeness and orthogonality relations for these eigenstates are

$$\sum_i |\vec{\phi}_i\rangle\langle\vec{\phi}_i| = \frac{\overset{\leftrightarrow}{1}}{\hat{\epsilon}_w},$$

$$\langle\vec{\phi}_i|\hat{\epsilon}_w|\vec{\phi}_j\rangle = \delta_{i,j}, \qquad (5)$$

where $\overset{\leftrightarrow}{1}$ is the unit tensor and $\delta_{i,j}$ is the Kronecker delta function. The sum over i in Eq. (5) is over all possible (physical and unphysical) solutions of Eq. (4).

We formulate a Green's function solution to Eq. (3) based on the full Green's function $\hat{G}$, characteristic of a PC containing both the 1D and 0D defects:

$$|\vec{\Psi}\rangle = |\vec{\Psi}^{hom}\rangle + 4\pi\widetilde{\omega}^2 \hat{G}\hat{\chi}^{0D}|\vec{\Psi}^{hom}\rangle, \qquad (6)$$

where $|\vec{\Psi}^{hom}\rangle$, the homogeneous solution, is an eigenstate of the system defined by Eq. (4). Green's function $\overset{\leftrightarrow}{G}(\vec{r},\vec{r}') = \langle\vec{r}|\hat{G}|\vec{r}'\rangle$ is defined by the equation

$$(\mathcal{L} - \widetilde{\omega}^2\hat{\epsilon}_w - 4\pi\widetilde{\omega}^2\hat{\chi}^{0D})\hat{G} = (\mathcal{L} - \widetilde{\omega}^2\hat{\epsilon}_t)\hat{G} = \overset{\leftrightarrow}{1}. \qquad (7)$$

The solution for the electric field of the coupled waveguide-cavity PC is then reduced to finding Green's function that satisfies Eq. (7) and using it to solve Eq. (6).

B. Green's function

A simple analytic solution of this problem, valid in the limit of weak coupling, can be obtained by expanding $\hat{G}$ in terms of a restricted set of intuitively chosen basis states. Quite generally, $\hat{G}$ can be uniquely expanded in terms of any orthonormal basis $\{|\vec{\phi}_n\rangle\}$ as

$$\hat{G} = \sum_{n,m} b_{n,m}|\vec{\phi}_n\rangle\langle\vec{\phi}_m|, \qquad (8)$$

where both sums extend over all states in the basis. We assume that the cavity introduced by $\hat{\chi}^{0D}$ would, in the absence of the 1D waveguide, support only one 0D localized mode. This mode is at a frequency $\widetilde{\omega}_l$, and is denoted by the eigenket $|\vec{\phi}_l\rangle$. Defining $\epsilon_d(\vec{r}) = \epsilon_t(\vec{r}) - 4\pi\chi^{1D}(\vec{r})$ as a dielectric function that describes the background PC and just the 0D cavity, the homogeneous equation that the localized state satisfies is

$$\mathcal{L}|\vec{\phi}_l\rangle = \widetilde{\omega}_l^2 \hat{\epsilon}_d |\vec{\phi}_l\rangle. \qquad (9)$$

It follows that the localized state is normalized as $\langle\vec{\phi}_l|\hat{\epsilon}_d|\vec{\phi}_l\rangle = 1$.

We also assume that in the absence of the 0D defect, $\hat{\chi}^{1D}$ supports only one band of 1D waveguide modes, labeled k_i, in the frequency range of interest. The subscript i runs from 0 to ∞, representing the infinite number of distinct wave vectors of the 1D guided modes, denoted by $|\vec{\phi}_{k_i}\rangle$. These are solutions of Eq. (4).

The localized mode eigenstate $\vec{\phi}_l(\vec{r})$ is normalized as follows:

$$\vec{\phi}_l(\vec{r}) = \frac{1}{\sqrt{V_{mode}}}\vec{v}_l(\vec{r}), \qquad (10)$$

where $\vec{v}_l(\vec{r})$ is a unitless function that describes the shape of the localized eigenstate. It might be obtained from a FDTD calculation, for example. The effective mode volume V_{mode} is given by the normalization condition following Eq. (9):

$$V_{mode} = \int_{all\ space} d\vec{r}\,\epsilon_d(\vec{r})|\vec{v}_l(\vec{r})|^2. \qquad (11)$$

To be consistent with earlier definitions of the mode volume we assume that the maximum of the product $\epsilon_d(\vec{r})|\vec{v}_l(\vec{r})|^2$ is scaled to unity.

For the guided mode it is natural to express the orthonormal states as

$$\vec{\phi}_{k_i}(\vec{r}) = \frac{1}{\sqrt{A_{eff}L}}\vec{u}_{k_i}(\vec{r})e^{ik_i x}, \qquad (12)$$

where $\vec{u}_{k_i}(\vec{r}) = \vec{u}_{k_i}(\vec{r} + \Lambda\hat{x})$ is a unitless Bloch function periodic along the direction of the waveguide, L is the length of the guide, and A_{eff} is an effective area of the mode. Substituting this form for $\vec{\phi}_{k_i}(\vec{r})$ into the orthogonality relation for the guided modes, and converting the integral over all space to the one over a unit cell by multiplying by $N = L/\Lambda$, the number of unit cells, one finds

$$A_{eff} = \frac{1}{\Lambda} \int_{unit\ cell} d\vec{r}\, \epsilon_w(\vec{r}) |\vec{u}_{k_i}(\vec{r})|^2, \qquad (13)$$

where the maximum of $\epsilon_w(\vec{r})|\vec{u}_{k_i}(\vec{r})|^2$ is scaled to unity.

If these 1D and 0D defect modes all exist well within the photonic band gap of the host PC, then it is a good approximation to neglect all propagating, bulk PC modes in the expansion of $\hat{G}$. Because $|\vec{\phi}_{k_i}\rangle$ and $|\vec{\phi}_l\rangle$ are solutions of *different* wave equations, they are not strictly orthogonal. Neglecting this for the moment, we proceed by expanding $\hat{G}$, using Eq. (8), in terms of $|\vec{\phi}_l\rangle$ and $\{|\vec{\phi}_{k_i}\rangle\}$. Substituting this expansion into the defining equation (7), and projecting onto the state $\langle \vec{\phi}_i|$ from the left and $\hat{\epsilon}_t |\vec{\phi}_j\rangle$ from the right, we find

$$\sum_{n,m} [\tilde{\omega}_n^2 \langle \vec{\phi}_i|\hat{\epsilon}_n|\vec{\phi}_n\rangle - \tilde{\omega}^2 \langle \vec{\phi}_i|\hat{\epsilon}_t|\vec{\phi}_n\rangle] b_{n,m} \langle \vec{\phi}_m|\hat{\epsilon}_t|\vec{\phi}_j\rangle$$

$$= \langle \vec{\phi}_i|\hat{\epsilon}_t|\vec{\phi}_j\rangle, \qquad (14)$$

where here the subscripts i and j refer to any state n in our basis. In the first term, $\hat{\epsilon}_n = \hat{\epsilon}_w$ if $n=\{k_i\}$ corresponding to a waveguide mode, and $\hat{\epsilon}_n = \hat{\epsilon}_d$ if $n=l$, corresponding to the 0D localized mode.

Equation (14) can be written in matrix form as follows:

$$\overset{\leftrightarrow}{M}\, \vec{b}\, \overset{\leftrightarrow}{T} = \overset{\leftrightarrow}{T}. \qquad (15)$$

For the physical scattering problem of interest here, $\vec{T}$ will have an inverse, so the expansion coefficients of $\hat{G}$ are given by

$$b_{n,m} = [M^{-1}]_{n,m} = \frac{\Delta_{m,n}}{\det(M)} \qquad (16)$$

where $\det(M)$ is the determinant of matrix M and $\Delta_{m,n}$ is the cofactor of element $M_{m,n}$. Directly from Eq. (14), the elements of matrix M are

$$M_{m,n} = \tilde{\omega}_n^2 \langle \vec{\phi}_m|\hat{\epsilon}_w|\vec{\phi}_n\rangle - \tilde{\omega}^2 \langle \vec{\phi}_m|\hat{\epsilon}_t|\vec{\phi}_n\rangle, \qquad (17)$$

for $n \neq l$ and

$$M_{m,l} = \tilde{\omega}_l^2 \langle \vec{\phi}_m|\hat{\epsilon}_d|\vec{\phi}_l\rangle - \tilde{\omega}^2 \langle \vec{\phi}_m|\hat{\epsilon}_t|\vec{\phi}_l\rangle, \qquad (18)$$

for $n=l$. However, unitarity ($M_{k_i,l} = M_{l,k_i}^*$) requires that

$$\tilde{\omega}_l^2 \langle \vec{\phi}_{k_i}|\epsilon_d|\vec{\phi}_l\rangle = \tilde{\omega}_{k_i}^2 \langle \vec{\phi}_l|\epsilon_w|\vec{\phi}_{k_i}\rangle^* = \tilde{\omega}_{k_i}^2 \langle \vec{\phi}_{k_i}|\epsilon_w|\vec{\phi}_l\rangle, \qquad (19)$$

which means that there is in fact no distinction to be made for $n=l$, except for the diagonal $n=m=l$ term, which does require the distinct expression, Eq. (18).

The derivation to this point has only been restricted by the assumption that the guide and cavity support a single mode each, and that these modes are deep within a band gap so that coupling to bulk and radiation modes can be neglected. We now make some approximations characteristic of a weak coupling regime.

In the weak coupling regime the localized and guided eigenstates are only weakly perturbed by each other and therefore are themselves very close to being eigenstates of the full photonic crystal described by $\hat{\epsilon}_t$. Within this approximation it follows that our intuitive basis approximately satisfies the following orthogonality relation:

$$\langle \vec{\phi}_n|\hat{\epsilon}_t|\vec{\phi}_m\rangle = \delta_{n,m}. \qquad (20)$$

In the Appendix we present a further justification of this approximation.

Using Eq. (20), the matrix elements of M can be expressed as

$$M_{m,n} = \tilde{\omega}_n^2 \langle \vec{\phi}_m|\hat{\epsilon}_w|\vec{\phi}_n\rangle - \tilde{\omega}^2 \delta_{m,n} \qquad (21)$$

for all but the $n=m=l$ term, which is instead

$$M_{l,l} = \tilde{\omega}_l^2 \langle \vec{\phi}_l|\hat{\epsilon}_d|\vec{\phi}_l\rangle - \omega^2. \qquad (22)$$

Making use of the rigorous orthogonality condition for the guided modes, as well as the normalization condition for the localized state, we arrive at

$$M_{m,n} = (\tilde{\omega}_n^2 - \tilde{\omega}^2)\delta_{m,n} \qquad (23)$$

for $n,m \neq l$,

$$M_{l,l} = \tilde{\omega}_l^2 - \tilde{\omega}^2, \qquad (24)$$

and

$$M_{k_i,l} = M_{l,k_i}^* = -4\pi \tilde{\omega}_{k_i}^2 \langle \vec{\phi}_{k_i}|\hat{\chi}^{0D}|\vec{\phi}_l\rangle, \qquad (25)$$

where we have used the definition of $\hat{\epsilon}_w$, and the approximate orthogonality between the localized and guided mode in deriving Eq. (25) from Eq. (21). The overlap function $\chi_{k_i,l}^{0D}$ is defined as

$$\chi_{k_i,l}^{0D} = \langle \vec{\phi}_{k_i}|\hat{\chi}^{0D}|\vec{\phi}_l\rangle = \int d\vec{r}\, \chi^{0D}(\vec{r})\vec{\phi}_{k_i}^*(\vec{r}) \cdot \vec{\phi}_l(\vec{r}). \qquad (26)$$

If we adopt an indexing convention for the basis states where the localized mode is labeled 1, then the matrix M has a dense first row and column followed by an infinite diagonal block.

This concludes the derivation of the Green's function. It is valid within the weak coupling approximation, and only applies when the guide and cavity each support a single mode deep within a band gap defined by the surrounding PC.

C. Guided mode expansion coefficients

The solution to the wave equation can now be expressed as

$$|\vec{\Psi}\rangle = |\vec{\Psi}^{hom}\rangle + \sum_{n,m} 4\pi\widetilde{\omega}^2 [M^{-1}]_{n,m} |\vec{\phi}_n\rangle \langle \vec{\phi}_m | \hat{\chi}^{0D} | \vec{\Psi}^{hom}\rangle, \tag{27}$$

which suggests that $|\vec{\Psi}\rangle = \Sigma_i a_i(\widetilde{\omega}) |\vec{\phi}_i\rangle$, where the subscript i can be any one of $\{i\} = \{l, k_1, k_2, \ldots\}$. If the homogeneous field is expressed as $|\vec{\Psi}^{hom}\rangle = a_h |\vec{\phi}_{k_h}\rangle$, then the expansion coefficient of an arbitrary waveguide mode is given by

$$a_{k_i}(\widetilde{\omega}) = a_h \delta_{k_i,k_h} + \sum_m 4\pi\widetilde{\omega}^2 [M^{-1}]_{k_i,m} \langle \vec{\phi}_m | \hat{\chi}^{0D} | \vec{\phi}_{k_h}\rangle a_h. \tag{28}$$

Due to the block diagonal form of M the only nonzero

term in the sum over m in Eq. (28) is for $m = l$. The coefficient $[M^{-1}]_{k_i,l}$ is

$$[M^{-1}]_{k_i,l} = \frac{(-1)^{l+k_i}\det(M_{l,k_i})}{\det(M)}$$

$$= \frac{\sum_{n \neq k_i} (-1)^{l+k_i}(-1)^{1+n+k_i} M_{k_i,n}\det(M_{k_i,n/l,k_i})}{\det(M)}, \tag{29}$$

where the factors of (-1) in the second equality are for $k_i > l$ and $n < k_i$. As above, only the $n = l$ term contributes to this sum. The $\det(M_{k_i,l/l,k_i})$ term represents the determinant of a diagonal matrix and is therefore given by the product of the diagonal elements. Thus Eq. (28) becomes

$$a_{k_i}(\widetilde{\omega}) = a_h \delta_{k_i,k_h} + \frac{(4\pi)^2 \widetilde{\omega}^2 \widetilde{\omega}_{k_i}^2 \langle \vec{\phi}_{k_i} | \hat{\chi}^{0D} | \vec{\phi}_l \rangle \langle \vec{\phi}_l | \hat{\chi}^{0D} | \vec{\phi}_{k_h}\rangle a_h \Pi_{n \neq l,k_i}(\widetilde{\omega}_n^2 - \widetilde{\omega}^2)}{\det(M)}. \tag{30}$$

The determinant of M can be written as

$$\det(M) = M_{l,l}\det(M_{l,l}) - \sum_{i \neq l} (1)^i M_{l,i}\det(M_{l,i}) = M_{l,l}\det(M_{l,l}) - \sum_{i,j \neq l} (-1)^{i+j} M_{l,i} M_{j,l}\det(M_{j,l/l,i}). \tag{31}$$

The subdeterminant $\det(M_{j,l/l,i})$ is nonzero only when $j = i$ due to the diagonal form of the waveguide eigenstate block in M. The subdeterminants in Eq. (31) are just the product of the remaining diagonals and therefore we have

$$\det(M) = \Pi_{i \neq l}(\widetilde{\omega}_i^2 - \widetilde{\omega}^2)\left[\widetilde{\omega}_l^2 - \widetilde{\omega}^2 - \sum_{i \neq l} (4\pi)^2 \widetilde{\omega}_i^4 \frac{\langle \vec{\phi}_l | \hat{\chi}^{0D} | \vec{\phi}_i \rangle \langle \vec{\phi}_i | \hat{\chi}^{0D} | \vec{\phi}_l \rangle}{\widetilde{\omega}_i^2 - \widetilde{\omega}^2}\right]. \tag{32}$$

The expansion coefficient we seek is then

$$a_{k_i}(\widetilde{\omega}) = a_h \delta_{k_i,k_h} + \frac{\dfrac{(4\pi)^2 \widetilde{\omega}^2 \widetilde{\omega}_{k_i}^2 \langle \vec{\phi}_{k_i} | \hat{\chi}^{0D} | \vec{\phi}_l \rangle \langle \vec{\phi}_l | \hat{\chi}^{0D} | \vec{\phi}_{k_h}\rangle a_h}{(\widetilde{\omega}_{k_i}^2 - \widetilde{\omega}^2)}}{\widetilde{\omega}_l^2 - \widetilde{\omega}^2 - \sum_{i \neq l} (4\pi)^2 \widetilde{\omega}_i^4 \dfrac{\langle \vec{\phi}_l | \hat{\chi}^{0D} | \vec{\phi}_i \rangle \langle \vec{\phi}_i | \hat{\chi}^{0D} | \vec{\phi}_l \rangle}{\widetilde{\omega}_i^2 - \widetilde{\omega}^2}}. \tag{33}$$

Since the sum over i in Eq. (33) does not include the localized state l, we can specify $\Sigma_i \to \Sigma_{k_i}$. This sum, evaluated by converting the sum to an integral, yields

$$a_{k_i}(\widetilde{\omega}) = a_h \delta_{k_i,k_h} + \frac{\dfrac{(4\pi)^2 \widetilde{\omega}^2 \widetilde{\omega}_{k_i}^2 \chi_{k_i,l}^{0D} \chi_{l,k_h}^{0D} a_h}{(\widetilde{\omega}_{k_i}^2 - \widetilde{\omega}^2)}}{\widetilde{\omega}_l^2 - \widetilde{\omega}^2 - \dfrac{i4\pi^2\widetilde{\omega}^3 L}{\widetilde{v}_g}[\chi_{+k_\omega,l}^{0D}\chi_{l,+k_\omega}^{0D} + \chi_{-k_\omega,l}^{0D}\chi_{l,-k_\omega}^{0D}]} \tag{34}$$

as the final expression for the expansion coefficient.

D. Localized mode amplitude

Although not needed to calculate the reflection and transmission of the guided mode in the linear response regime, the amplitude of the localized mode is important when deriving the nonlinear response in the cavity. The amplitude coefficient of the localized mode is, from Eq. (27),

$$a_l(\widetilde{\omega}) = \sum_m 4\pi\widetilde{\omega}^2 [M^{-1}]_{l,m} \langle \vec{\phi}_m | \hat{\chi}^{0D} | \vec{\phi}_{k_h} \rangle a_h. \quad (35)$$

The only nonzero term in the sum is again $m=l$. The required element of M^{-1} is

$$[M^{-1}]_{l,l} = \frac{\det(M_{l,l})}{\det(M)} = \frac{\Pi_{i \neq l}(\widetilde{\omega}_i^2 - \widetilde{\omega}^2)}{\det(M)}, \quad (36)$$

where $\det(M)$ is given in Eq. (32).

After evaluating the sums in the denominator as in the preceding section, we find

$$a_l(\widetilde{\omega}) = \frac{4\pi\widetilde{\omega}^2 \chi_{l,k_h}^{0D} a_h}{\widetilde{\omega}_l^2 - \widetilde{\omega}^2 - \dfrac{i4\pi^2\widetilde{\omega}^3 L}{\widetilde{v}_g} [\chi_{+k_\omega,l}^{0D} \chi_{l,+k_\omega}^{0D} + \chi_{-k_\omega,l}^{0D} \chi_{l,-k_\omega}^{0D}]}. \quad (37)$$

E. Reflected and transmitted fields

The transmitted field is found by evaluating the fields at $x = +\infty$. Only the waveguide modes carry energy far away from the localized defect, hence we need only sum over the k_i states in our basis:

$$\langle x \to \infty | \vec{\Psi} \rangle = \sum_{k_i} a_{k_i}(\widetilde{\omega}) \langle x \to \infty | \vec{\phi}_{k_i} \rangle. \quad (38)$$

The sum over k_i is similar to the one that appeared in the denominator above; however, now there is an exponential factor $e^{ik_i x}$ coming from the eigenstate $\langle \vec{r} | \vec{\phi}_{k_i} \rangle$. Assuming that both the Bloch function of the eigenstate and the overlap integrals vary slowly with the in-plane momentum k_i, the integral reduces to

$$\frac{L}{2\pi} \frac{1}{2\widetilde{\omega}\widetilde{v}_g} \int dk_i \widetilde{\omega}_{k_i}^2 \left[\frac{e^{ik_i x}}{k_i - k_\omega - i\epsilon} - \frac{e^{ik_i x}}{k_i + k_\omega + i\epsilon} \right]$$

$$= \frac{L}{4\pi\widetilde{\omega}\widetilde{v}_g} [2\pi i\, \theta(x) e^{ik_\omega x} \mathcal{R}(k_\omega)$$

$$+ 2\pi i\, \theta(-x) e^{-ik_\omega x} \mathcal{R}(-k_\omega)], \quad (39)$$

where θ is the step function and $\mathcal{R}(k_\omega)$ is the residue of the integral evaluated at k_ω. Carrying out the integrals, we find

$$\langle x \to \infty | \vec{\Psi} \rangle = \left[1 + \frac{\dfrac{i8\pi^2\widetilde{\omega}^3 L}{\widetilde{v}_g} \chi_{k_\omega,l}^{0D} \chi_{l,k_\omega}^{0D}}{\widetilde{\omega}_l^2 - \widetilde{\omega}^2 - \dfrac{i4\pi^2\widetilde{\omega}^3 L}{\widetilde{v}_g} [\chi_{+k_\omega,l}^{0D} \chi_{l,+k_\omega}^{0D} + \chi_{-k_\omega,l}^{0D} \chi_{l,-k_\omega}^{0D}]} \right] a_h \langle x \to \infty | \vec{\phi}_{k_\omega} \rangle, \quad (40)$$

where we have taken the in-plane momentum of the homogeneous field to be $+k_\omega$, a forward propagating guided mode.

The field at $x \to -\infty$ is

$$\langle x \to -\infty | \vec{\Psi} \rangle = \langle \vec{r} | \vec{\Psi}_{inc} \rangle + \langle \vec{r} | \vec{\Psi}_{ref} \rangle$$

$$= \sum_{k_i} a_{k_i}(\widetilde{\omega}) \langle x \to -\infty | \vec{\phi}_{k_i} \rangle$$

$$= a_h \langle x \to -\infty | \vec{\phi}_{k_\omega} \rangle + \frac{\dfrac{i8\pi^2\widetilde{\omega}^3 L}{\widetilde{v}_g} \chi_{-k_\omega,l}^{0D} \chi_{l,k_\omega}^{0D}}{\widetilde{\omega}_l^2 - \widetilde{\omega}^2 - \dfrac{i4\pi^2\widetilde{\omega}^3 L}{\widetilde{v}_g} [\chi_{+k_\omega,l}^{0D} \chi_{l,+k_\omega}^{0D} + \chi_{-k_\omega,l}^{0D} \chi_{l,-k_\omega}^{0D}]} a_h \langle x \to -\infty | \vec{\phi}_{-k_\omega} \rangle. \quad (41)$$

Invoking a mirror symmetry of the 0D defect structure along the waveguide axis, we can set the overlap integrals involving $+k_\omega$ equal to those involving $-k_\omega$. That is, $\langle \vec{\phi}_{-k_\omega} | \hat{\chi}^{0D} | \vec{\phi}_l \rangle = \langle \vec{\phi}_{+k_\omega} | \hat{\chi}^{0D} | \vec{\phi}_l \rangle$. The transmission and reflection coefficients are then

$$T(\omega) = \frac{\langle x \rightarrow \infty | \vec{\Psi} \rangle}{a_h \langle x \rightarrow \infty | \vec{\phi}_{+k_\omega} \rangle}$$

$$= 1 + \frac{\dfrac{i 8 \pi^2 \tilde{\omega}^3 L}{\tilde{v}_g} \chi^{0D}_{w,l} \chi^{0D}_{l,w}}{\tilde{\omega}_l^2 - \tilde{\omega}^2 - \dfrac{i 8 \pi^2 \tilde{\omega}^3 L}{\tilde{v}_g} \chi^{0D}_{w,l} \chi^{0D}_{l,w}} \qquad (42)$$

and

$$R(\omega) = \frac{\langle x \rightarrow -\infty | \vec{\Psi}_{ref} \rangle}{a_h \langle x \rightarrow -\infty | \vec{\phi}_{-k_\omega} \rangle}$$

$$= \frac{\dfrac{i 8 \pi^2 \tilde{\omega}^3 L}{\tilde{v}_g} \chi^{0D}_{w,l} \chi^{0D}_{l,w}}{\tilde{\omega}_l^2 - \tilde{\omega}^2 - \dfrac{i 8 \pi^2 \tilde{\omega}^3 L}{\tilde{v}_g} \chi^{0D}_{w,l} \chi^{0D}_{l,w}}, \qquad (43)$$

where the subscript w simply denotes the waveguide mode at frequency $\tilde{\omega}$.

Before generalizing this solution to include downstream reflections and a third-order nonlinear response, we compare our derivation in the linear response regime with those previously published by others.

Equations (43) and (42) are, respectively, the reflection and transmission of a guided mode that is weakly coupled to an otherwise lossless resonant cavity. The line shape is Lorentzian,

$$R(\tilde{\omega}) = \frac{i \tilde{\omega} \Gamma}{\tilde{\omega}_l^2 - \tilde{\omega}^2 - i \tilde{\omega} \Gamma}, \qquad (44)$$

with a linewidth of

$$\Gamma = \frac{8 \pi^2 \tilde{\omega}^2 L |\chi^{0D}_{w,l}|^2}{\tilde{v}_g}. \qquad (45)$$

Note that the Q of the resonance is given by $Q = \tilde{\omega}_l / \Gamma$.

Our result is a direct solution of the wave equation and has involved approximations that are physically justified if the guide and cavity are weakly coupled. If the denominator is appropriately factorized, Eq. (44) has exactly the same form as in Ref. [3], with the exception that our overlap function $\chi^{0D}_{l,w}$ is well defined in terms of overlap integrals involving eigenmodes and the dielectric perturbation that defines the 0D cavity. In the Hamiltonian formulation of this scattering problem, the corresponding coupling term is given in terms of the difference between a dielectric function $\epsilon_o(\vec{r})$ "associated with the unperturbed Hamiltonian," and the total dielectric function $\epsilon_t(\vec{r})$. However, the "unperturbed" dielectric function $\epsilon_o(\vec{r})$ is ill defined, since there is no unique dielectric function that at once has the waveguide and localized modes as exact solutions.

Our derivation actually sheds some light on the resolution of this ambiguity. If Eqs. (17) and (18), as well as the orthogonality condition of Eq. (20), are used in the remainder of the development, without invoking the unitarity condition, Eq. (19), then the final solution does not conserve flux. Within the weak coupling approximation then, it is necessary to adopt Eq. (19) to conserve flux. When comparing our unitary result with that derived in Ref. [3], it becomes clear that $\epsilon_o(\vec{r})$ can be taken as *either* our $\epsilon_w(\vec{r})$ or our $\epsilon_d(\vec{r})$ in order to obtain a physically well-defined coupling matrix element.

F. Nonresonant background

We now modify the geometry in order to treat the more general situation when there is some downstream perturbation of the 1D waveguide that introduces a frequency-dependent (linear) background reflectivity $\mathcal{R}_{nr}$, which we assume is known. This background reflectivity is incorporated in a manner consistent with our Green's function formulation of the scattering problem: Fan [25] has previously used a transfer matrix approach to include the effects of downstream reflection on linear resonator-waveguide coupling.

The full expression for the field in the waveguide plus cavity system, before taking the asymptotic limit to $x = -\infty$, which yields the reflectivity, and before any of the sums over k_i are carried out, is given by

$$|\vec{\Psi}\rangle = \sum_{k_i} a_{k_i} |\vec{\phi}_{k_i}\rangle + a_l |\vec{\phi}_l\rangle$$

$$= a_h |\vec{\phi}_{k_h}\rangle + \frac{(4\pi)^2 \tilde{\omega}^2 \displaystyle\sum_{k_i} \tilde{\omega}_{k_i}^2 \dfrac{|\vec{\phi}_{k_i}\rangle \langle \vec{\phi}_{k_i} | \hat{\chi}^{0D} | \vec{\phi}_l \rangle \langle \vec{\phi}_l | \hat{\chi}^{0D} | \vec{\phi}_{k_h} \rangle a_h}{\tilde{\omega}_{k_i}^2 - \tilde{\omega}^2} + 4\pi \tilde{\omega}^2 |\vec{\phi}_l\rangle \langle \vec{\phi}_l | \hat{\chi}^{0D} | \vec{\phi}_{k_h} \rangle a_h}{\tilde{\omega}_l^2 - \tilde{\omega}^2 - \displaystyle\sum_{k_i} (4\pi)^2 \tilde{\omega}_{k_i}^4 \dfrac{\langle \vec{\phi}_l | \hat{\chi}^{0D} | \vec{\phi}_{k_i} \rangle \langle \vec{\phi}_{k_i} | \hat{\chi}^{0D} | \vec{\phi}_l \rangle}{\tilde{\omega}_{k_i}^2 - \tilde{\omega}^2}}, \qquad (46)$$

which can be written in operator notation as

$$|\vec{\Psi}\rangle = a_h|\vec{\phi}_{k_h}\rangle + \frac{\hat{G}_o\hat{V}|\vec{\phi}_l\rangle\langle\vec{\phi}_l|\hat{V}|\vec{\phi}_{k_h}\rangle a_h + |\vec{\phi}_l\rangle\langle\vec{\phi}_l|\hat{V}|\vec{\phi}_{k_h}\rangle a_h}{\widetilde{\omega}_l^2 - \widetilde{\omega}^2 - \langle\vec{\phi}_l|\hat{V}\hat{G}_o\hat{V}|\vec{\phi}_l\rangle}.$$

(47)

The operator $\hat{V}$, with matrix element $\langle\vec{\phi}_l|\hat{V}|\vec{\phi}_{k_i}\rangle = 4\pi\widetilde{\omega}_{k_i}^2\langle\vec{\phi}_l|\hat{\chi}^{0D}|\vec{\phi}_{k_i}\rangle$ (note $\widetilde{\omega}_{k_h} = \widetilde{\omega}$), is defined to conveniently group factors associated with the driving term in a Green's function solution. The operator $\hat{G}_o$ is defined as $\hat{G}_o = \Sigma_{k_i}|\vec{\phi}_{k_i}\rangle\langle\vec{\phi}_{k_i}|/(\widetilde{\omega}_{k_i}^2 - \widetilde{\omega}^2)$. In the regime where contributions from nonguided modes of the 1D waveguide PC can be neglected, the sum over k_i can be taken to be the sum over all eigenmodes of the waveguide PC. Therefore the operator $\hat{G}_o$ is just the bare Green's function of the 1D waveguide PC.

From Eq. (47) it is evident that the full electric field depends on a bare Green's function $\hat{G}_o$ and a corresponding homogeneous field $|\vec{\phi}_{k_h}\rangle$, both characteristic of the exact structure of interest, minus the local mode whose resonant coupling is being sought. To generalize our previous result, we therefore seek the homogeneous solutions and corresponding bare Green's function characteristic of the 1D waveguide *including* the downstream perturbation, but *excluding* the perturbation responsible for the local mode of interest to us. These will be substituted in place of the Green's function and the homogeneous field presently used in Eq. (47). This approach is valid as long as the nonresonant

source does not alter the operator $\hat{\chi}^{0D}$. Therefore, the nonresonant source must be external to the cavity.

The new Green's function and homogeneous field are found as follows. Assume the source of the nonresonant background is described by some susceptibility $\hat{\chi}_{nr}$. The wave equation is

$$(\mathcal{L} - \widetilde{\omega}^2\hat{\epsilon}_w)|\vec{\Psi}_{nr}\rangle = 4\pi\widetilde{\omega}^2\hat{\chi}_{nr}|\vec{\Psi}_{nr}\rangle.$$

(48)

The subscript nr serves to make it explicit that this is the electric field of a waveguide PC with a nonresonant source, not the full electric field as in Eq. (47). The Green's function solution is

$$|\vec{\Psi}_{nr}\rangle = (1 + 4\pi\widetilde{\omega}^2\hat{G}_{nr}\hat{\chi}_{nr})|\vec{\Psi}_h\rangle.$$

(49)

Defining $\hat{N} = 4\pi\widetilde{\omega}^2\hat{G}_{nr}\hat{\chi}_{nr}$, Eq. (49) becomes

$$|\vec{\Psi}_{nr}\rangle = (1 + \hat{N})|\vec{\Psi}_h\rangle.$$

(50)

Furthermore, the Green's function for the full waveguide plus nonresonant perturbation is related to the Green's function of the 1D waveguide by Dyson's equation,

$$\hat{G}_{nr} = (1 + \hat{N})\hat{G}_o.$$

(51)

The nonresonant background can then be included in our solution by simply substituting $|\vec{\phi}_{k_h}\rangle \rightarrow (1 + \hat{N})|\vec{\phi}_{k_h}\rangle$ and $\hat{G}_o \rightarrow (1 + \hat{N})\hat{G}_o$ in Eq. (47). The field in the coupled waveguide-cavity system, with some nonresonant background present, is then

$$|\vec{\Psi}\rangle = (1+\hat{N})a_h|\vec{\phi}_{k_h}\rangle + \frac{(1+\hat{N})\hat{G}_o\hat{V}|\vec{\phi}_l\rangle\langle\vec{\phi}_l|\hat{V}(1+\hat{N})|\vec{\phi}_{k_h}\rangle a_h + |\vec{\phi}_l\rangle\langle\vec{\phi}_l|\hat{V}(1+\hat{N})|\vec{\phi}_{k_h}\rangle a_h}{\widetilde{\omega}_l^2 - \widetilde{\omega}^2 - \langle\vec{\phi}_l|\hat{V}(1+\hat{N})\hat{G}_o\hat{V}|\vec{\phi}_l\rangle}.$$

(52)

At a spatial location $\vec{r}$, upstream from the nonresonant scattering source—that is, $x < x_{nr}$, where x_{nr} is the spatial coordinate at which the nonresonant scattering source begins—the operator $\hat{N}$ acts on an eigenstate of the waveguide in the following way:

$$\langle\vec{r}(x<x_{nr})|\hat{N}|\vec{\phi}_{k_i}\rangle = \mathcal{R}_{nr}(\widetilde{\omega}_{k_i},x)\vec{\phi}_{-k_i}(\vec{r}),$$

(53)

where $\mathcal{R}_{nr}(\widetilde{\omega}_{k_i},x)$ is a complex scalar function of k_i and position x. This is nothing more than the definition of a reflection coefficient for the guided mode reflecting from the nonresonant source. In the present context we are only concerned with the value of the reflection coefficient at $x = x_o$, the location of the resonant cavity; thus we define $\mathcal{R}_{nr}(\widetilde{\omega}_{k_i},x_o) = R_{nr}(\widetilde{\omega}_{k_i})$.

With this definition of the operator $\hat{N}$, the evaluation of the sums, and of the fields at $x = -\infty$, follows the approach already presented. The result, for the reflectivity of a guided

mode coupled via $\hat{\chi}^{0D}$ to a resonant cavity and scattered by a downstream perturbation with reflectivity $R_{nr}(\widetilde{\omega})$, is

$$R(\omega) = R_{nr}(\widetilde{\omega})$$

$$+ \frac{\dfrac{i8\pi^2\widetilde{\omega}^3 L}{\widetilde{v}_g}[1 + R_{nr}(\widetilde{\omega})]^2\chi_{w,l}^{0D}\chi_{l,w}^{0D}}{\widetilde{\omega}_l^2 - \widetilde{\omega}^2 - \dfrac{i8\pi^2\widetilde{\omega}^3 L}{\widetilde{v}_g}[1 + R_{nr}(\widetilde{\omega})]\chi_{w,l}^{0D}\chi_{l,w}^{0D}},$$

(54)

which has the simple form of a renormalized Lorentzian line shape coherently added to a nonresonant background. Owing to the interference of the downstream and resonant contributions, the line shape of the resonance in the reflection spectra is generally Fano-like.

Finally, from Eq. (52), the amplitude of the localized mode is found to be

$$a_l(\widetilde{\omega}) = \frac{4\pi\widetilde{\omega}^2 \chi^{0D}_{l,k_h} a_h [1 + R_{nr}(\widetilde{\omega})]}{\widetilde{\omega}_l^2 - \widetilde{\omega}^2 - \dfrac{i8\pi^2\widetilde{\omega}^3 L}{\widetilde{v_g}} \chi^{0D}_{w,l} \chi^{0D}_{l,w} [1 + R_{nr}(\widetilde{\omega})]}.$$

(55)

This amplitude will be important for the nonlinear discussion in the following section.

III. COUPLED WAVEGUIDE AND CAVITY IN NONLINEAR REGIME

In this section we show how the above solution may be extended to include a third-order nonlinear response of the host material.

A general nonlinear polarization $|\vec{P}^{NL}\rangle$ is included by modifying Eq. (3) as

$$(\mathcal{L} - \widetilde{\omega}^2 \hat{\epsilon}_w) |\vec{\Psi}\rangle = 4\pi\widetilde{\omega}^2 \hat{\chi}^{0D} |\vec{\Psi}\rangle + 4\pi\widetilde{\omega}^2 |\vec{P}^{NL}\rangle. \quad (56)$$

The third-order degenerate nonlinear polarization is given in real space by

$$\vec{P}^{NL}(\vec{r},\omega) = \tfrac{3}{2} \overleftrightarrow{\chi}^{(3)}(\vec{r}, -\omega; \omega, -\omega, \omega)$$

$$\times \vec{E}(\vec{r},\omega)\vec{E}^*(\vec{r},\omega)\vec{E}(\vec{r},\omega), \quad (57)$$

and by grouping terms it can be seen that the net physical effect of this nonlinearity is to introduce an intensity dependent susceptibility

$$\overleftrightarrow{\chi}^{NL}(\vec{r}) = \tfrac{3}{2} \overleftrightarrow{\chi}^{(3)}(\vec{r}) : \vec{E}(\vec{r})\vec{E}^*(\vec{r}). \quad (58)$$

Note that $\overleftrightarrow{\chi}^{(3)}$ is in general complex. The real part leads to an intensity dependent refractive index, while the imaginary part quantifies the amount of two-photon absorption.

In the weak coupling limit it is quite reasonable to assume that the only mode that will have enough intensity to induce a substantial nonlinear susceptibility will be the localized mode, when excited near resonance. Thus to a good approximation we can take

$$\overleftrightarrow{\chi}^{NL}(\vec{r}) = \tfrac{3}{2} \overleftrightarrow{\chi}^{(3)}(\vec{r}) : \vec{\phi}_l(\vec{r})\vec{\phi}_l^*(\vec{r}) |a_l(\widetilde{\omega})|^2$$

$$= \tfrac{3}{2} \overleftrightarrow{\chi}^{(3)}(\vec{r}) : \vec{v}_l(\vec{r})\vec{v}_l^*(\vec{r}) \frac{|a_l(\widetilde{\omega})|^2}{V_{mode}}. \quad (59)$$

From Eq. (59), $\overleftrightarrow{\chi}^{NL}(\vec{r})$ will, like $\overleftrightarrow{\chi}^{0D}(\vec{r})$, be localized in the vicinity of the defect mode, but it will not have exactly the same shape. In this formulation, it's dynamic behavior is determined completely by the localized mode amplitude $a_l(\widetilde{\omega})$. Equation (56) can thus be written as

$$(\mathcal{L} - \widetilde{\omega}^2 \hat{\epsilon}_w) |\vec{\Psi}\rangle = 4\pi\widetilde{\omega}^2 \{\hat{\chi}^{0D} + \hat{\chi}^{NL}[|a_l(\widetilde{\omega})|^2]\} |\vec{\Psi}\rangle. \quad (60)$$

Treating $|a_l(\widetilde{\omega})|^2$ as a parameter in $\hat{\chi}^{NL}$, as one might in an iterative solution to the nonlinear equation (60), one can formally replace $\hat{\chi}^{0D}$ with $\hat{\chi}^{0D} + \hat{\chi}^{NL}$ in all of the linear development presented above. Because the new expression largely preserves the local nature of $\hat{\chi}^{0D}$, the discussion of which matrix elements can be neglected due to the weak coupling approximation carries over, and further approximations can be made due to the relative size of $\hat{\chi}^{0D}$ and $\hat{\chi}^{NL}$. In particular, when considering different matrix elements $\langle \vec{\phi}_n | \hat{\chi}^{NL} | \vec{\phi}_m \rangle$, if n and m are both 1D guided modes, then the resulting overlap function describes a third order polarization generated from the evanescent tail of the guided mode. This is certainly negligible, given our approximation that only the field in the cavity is strong enough to generate a significant nonlinear polarization. If one of n or m is a localized mode and the other a guided mode, then the overlap function represents a nonlinear modification of the coupling to the localized mode and an associated modification of the resonant linewidth. While this is relevant, in the present analysis we only retain the largest effect of the nonlinearity, the direct renormalization of the resonant frequency of the bound mode through matrix elements of $\hat{\chi}^{NL}$ that involve the localized state twice.

With this assumption, the only element of M that is altered from those of the purely linear derivation is the $M_{l,l}$ element, which becomes $M_{l,l} = \widetilde{\omega}_l^2 - \widetilde{\omega}^2 - 4\pi\widetilde{\omega}^2 \chi^{NL}_{l,l}$, and this modification of M is the only change that is encountered in the linear analysis. Hence, the nonlinear reflectivity is given by

$$R(\omega) = R_{nr}(\widetilde{\omega})$$

$$+ \frac{i\widetilde{\omega}\Gamma(1 + R_{nr}(\widetilde{\omega}))^2}{\widetilde{\omega}_l^2 - \widetilde{\omega}^2 - 4\pi\widetilde{\omega}^2 \alpha |\mathcal{Q}|^2 - i\widetilde{\omega}\Gamma(1 + R_{nr}(\widetilde{\omega}))},$$

(61)

where we have written $\chi^{NL}_{l,l}$ as $\alpha |\mathcal{Q}|^2$. The coefficient α is defined as

$$\alpha = \frac{1}{V_{mode}} \frac{3}{2} \int d\vec{r} \vec{v}_l^*(\vec{r}) \cdot \overleftrightarrow{\chi}^{(3)}(\vec{r}) \vec{v}_l(\vec{r}) \vec{v}_l^*(\vec{r}) \vec{v}_l(\vec{r}), \quad (62)$$

which serves to separate the renormalized material response from the dynamical variable $\mathcal{Q} = a_l(\widetilde{\omega})/\sqrt{V_{mode}}$, associated with the localized mode amplitude.

Thus the modified $M_{l,l}$ element results in an extra factor in the denominator of the reflectivity that renormalizes the localized mode resonant frequency by an amount proportional to the intensity of the electric field in the cavity. Recall that formally we had to assume that the local mode amplitude was a parameter in our original equations of motion in order to obtain Eq. (61). To find the self-consistent value(s) of $a_l(\widetilde{\omega})$ that satisfy the full set of equations at a given frequency and incident field strength, we need to solve

$$a_l(\tilde{\omega}) = \frac{4\pi\tilde{\omega}^2 \chi_{l,w}^{0D} a_h [1 + R_{nr}(\tilde{\omega})]}{\tilde{\omega}_l^2 - \tilde{\omega}^2 - 4\pi\tilde{\omega}^2 \alpha \dfrac{|a_l(\tilde{\omega})|^2}{V_{mode}} - \dfrac{i8\pi^2\tilde{\omega}^3 L}{\tilde{v}_g} \chi_{w,l}^{0D} \chi_{l,w}^{0D} [1 + R_{nr}(\tilde{\omega})]}, \tag{63}$$

which is obtained by incorporating the modified $M_{l,l}$ matrix element in the derivation in Sec. II F.

Taking the amplitude squared of Eq. (63) results in a cubic equation whose roots are the values of $a_l(\tilde{\omega})$ that self-consistently solve our third-order nonlinear equation (63). These solutions are used in Eq. (61) to find the reflection spectra in the presence of the nonlinearity.

Finally, it is useful to express the amplitude of the homogeneous driving field, a_h, in terms of the average power of the incident waveguide mode. The total electromagnetic energy of the incident waveguide mode within one unit cell is

$$W = \frac{1}{2} \int_{unit\ cell} d\vec{r}\, [\epsilon_w(\vec{r})|\vec{E}_h(\vec{r})|^2 + |\vec{B}_h(\vec{r})|^2]$$

$$= \int_{unit\ cell} d\vec{r}\, \epsilon_w(\vec{r})|\vec{E}_h(\vec{r})|^2, \tag{64}$$

where $\vec{E}_h(\vec{r}) = a_h \vec{\phi}_{k_h}(\vec{r})$. The time for the energy to move from one unit cell to the next is $\Lambda/(\tilde{v}_g c)$, and therefore the power carried by the incident waveguide mode is $P = \tilde{v}_g c W/\Lambda$ or

$$P = \frac{\tilde{v}_g c}{\Lambda} |a_h|^2 \int_{unit\ cell} \frac{1}{A_{eff} L} \epsilon_w(\vec{r})|\vec{u}_{k_h}|^2 d\vec{r}$$

$$= \frac{\tilde{v}_g c}{L} |a_h|^2. \tag{65}$$

Thus, $a_h = \sqrt{LP/\tilde{v}_g c}$. Furthermore, from Eq. (45), $\chi_{l,w}^{0D} = \sqrt{\tilde{v}_g \Gamma/L 8\pi^2\tilde{\omega}^2}$, so Eq. (63) for $a_l(\tilde{\omega})$ can be reexpressed in terms of simple physical parameters as

$$a_l(\tilde{\omega}) = \frac{\tilde{\omega}\sqrt{2\Gamma P/c}[1 + R_{nr}(\tilde{\omega})]}{\tilde{\omega}_l^2 - \tilde{\omega}^2 - 4\pi\tilde{\omega}^2 \alpha \dfrac{|a_l(\tilde{\omega})|^2}{V_{mode}} - i\tilde{\omega}\Gamma(1 + R_{nr}(\tilde{\omega}))}. \tag{66}$$

Equations (61) and (66) represent the final result of our derivation. For a given incident power, the local mode amplitude in the cavity is obtained by solving Eq. (66) and the corresponding local field strength is $Q = a_l(\tilde{\omega})/\sqrt{V_{mode}}$. Equation (61) then yields the reflectivity of a waveguide mode, in a 1D waveguide PC, that interacts with a nonresonant scatterer *and* a localized nonlinear cavity that supports a single bound mode in the frequency range of interest.

Losses due to the nonlinear process of two-photon absorption are included in our formalism through a complex $\tilde{\chi}^{(3)}(\vec{r})$. If required, linear material losses could be included

by assuming a complex linear susceptibility. In any realistic structure there would be some radiation losses that would cause a finite resonant linewidth even in the limit of vanishingly small coupling between the waveguide and the cavity. This could be included in the formalism by including in our basis another set of modes with a continuous dispersion (in addition to the 1D waveguide modes treated above) and allowing them to couple to the localized mode. The net result would be an additional contribution to the linewidth $\Gamma \to \Gamma + \Gamma_o$ in the denominator of Eq. (61), with no corresponding change to the coupling [Γ in the numerator of Eq. (61) would remain unchanged]. This too is consistent with the linear result obtained using the Hamiltonian approach [3].

Finally, the general formalism presented above can be used to treat any order of nonlinear polarization. In practice, the approximations needed to render a simple analytical result, when possible, will depend on the nonlinearity considered.

IV. DISCUSSION

A. Nonlinear response

For the purpose of illustrating the nonlinear reflectivity properties of realistic PC waveguide structures, we adopt the set of material parameters summarized in Table I. The third-order susceptibility corresponds to a $Al_{0.18}Ga_{0.82}As$ host at a wavelength of 1.55 μm. We have neglected the order-unity renormalization to the bulk value of $\tilde{\chi}^{(3)}$ due to the nonuniform localized state. That is, over the extent of the localized mode we approximate $\alpha \approx \frac{3}{2}\chi^{(3)}(1/V_{mode})\int d\vec{r}|\vec{v}_l(\vec{r})|^4 \approx \frac{3}{2}\chi^{(3)}/\epsilon_{avg}^2$, where ϵ_{avg} is the average dielectric constant of the cavity region. A typical photonic crystal-based cavity could have an air to material filling fraction of roughly 30%. This leads to $\epsilon_{avg} = 8.11$ for an $Al_{0.18}Ga_{0.82}As$ index of 3.34. We focus on 18% $Al_x Ga_{1-x}As$ since it has been shown that it should have the greatest ratio of nonlinear refraction n_2 to two-photon absorption, β at 1.55 μm and is therefore of particular interest for optical switching applications [26,27]. Our value for the real part of $\chi^{(3)}$ (5.1×10^{-11} esu) can be found from the calculations and data presented in Ref. [26].

TABLE I. Material parameters used in simulations.

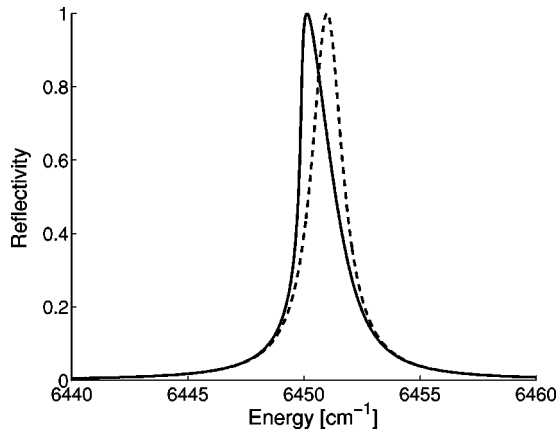| Parameter	Value	Units
$4\pi\alpha$	1.46×10^{-11}	esu
V_{mode}	0.055	μm^3
$\tilde{\omega}_l$	$\dfrac{2\pi}{1.55}$	μm^{-1}
Q	4000	None

FIG. 2. Reflection spectra for an incident mode power of 0.0021 mW (dashed) and 15.4 mW (solid). The plot at 0.0021 mW exactly coincides with the purely linear calculation, the plot of Eq. (44).

FIG. 3. Reflection spectra for incident mode powers of 2.2 mW (dotted), 44.0 mW (dashed), 87.6 mW (solid), and 131.6 mW (dash-dotted).

When the background, nonresonant reflectivity is ignored, the linear and the nonlinear reflectivity in this scattering geometry are essentially identical to the nonlinear transmission that has been studied extensively by others in the context of nonlinear 1D Fabry-Perot cavities [22,28]. Of significance here are the absolute powers required to observe bistable behavior in this PC geometry where the localized mode volume can be less than a cubic wavelength. We start by illustrating that Fabry-Perot-like bistable behavior can be observed at power levels as low as 40.0 mW in the structure described in Table I. The nontrivial influence of including downstream reflections will be considered next.

Figure 2 shows reflectivity spectra in the absence of any nonresonant background reflection for incident waveguide mode powers of 0.0021 mW (dashed curve) and 15.4 mW (solid curve). The dashed curve is the linear result that occurs when the peak field excited within the localized defect causes a negligible shift of the bound mode's resonant frequency. As the incident power is increased, the nonlinear term renormalizes the cavity mode resonance by an amount proportional to the renormalized susceptibility in the cavity region. As the energy approaches the resonance from below, the field strength in the cavity increases, which causes a nonlinear increase in the effective refractive index in the cavity region because the third-order susceptibility of $Al_xGa_{1-x}As$ is positive at 1.55 μm. The increase in the refractive index decreases the resonant mode frequency, pulling it towards the incident frequency which in turn further enhances the coupling to the cavity. This positive feedback increases the slope of the rising edge of the reflectivity spectrum as compared to the linear result. As the frequency extends beyond the renormalized resonant mode frequency the field amplitude in the cavity decreases and the mode shifts back towards its linear frequency. This negative feedback keeps the resonant frequency close to the incident guided mode frequency, resulting in a (relatively) shallow slope on the falling edge of the resonance.

The most interesting consequence of the Kerr-induced resonant frequency shift is the onset of bistability at higher powers. Figure 3 plots reflection spectra for incident powers up to 132.0 mW. In the current example the reflectivity be-
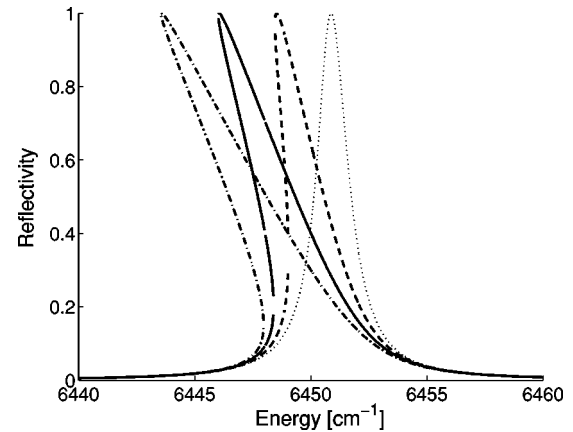
comes multivalued when the power is increased above $\sim$40.0 mW. This low threshold for bistability is a result of a large local field confined to a volume that is less than a cubic wavelength.

The curve of circles in Fig. 4 is a plot of the reflected power as a function of incident power at a fixed energy on the low energy side of the resonance. As the incident power is increased, the reflected power gradually increases along the bottom branch of the curve until it reaches about 155 mW. At this point, the reflected power jumps to around 70 mW due to the instability of the interior branch of the curve. Decreasing the incident power from above 155 mW, the reflected power follows the upper branch of the curve, dropping to minimal reflected power at about 55 mW. The dramatic variation from low to high reflected power, which corresponds to a switching from near zero to unity reflectivity, would be ideal for nonlinear switching applications. However, this simulation does not include the imaginary part of $\chi^{(3)}$, which accounts for two-photon absorption. When
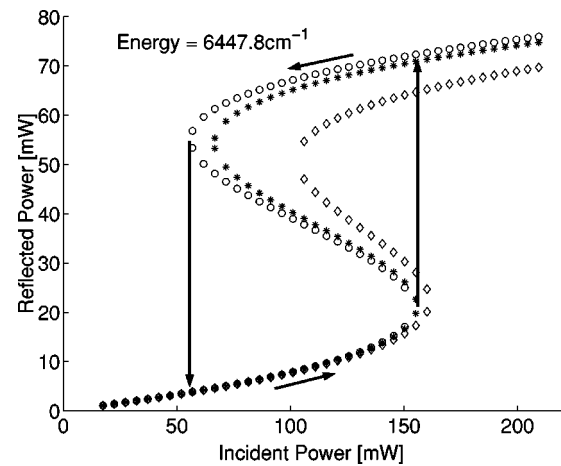

FIG. 4. Hysteresis loop for Lorentzian resonance at an energy of 6447.8 cm^{-1} (circles). The stars and diamonds show the effect of two-photon absorption (TPA) when the TPA coefficient is assumed to be 0.34 cm/GW and 1.46 cm/GW, respectively. The arrows indicate the bistable loop.
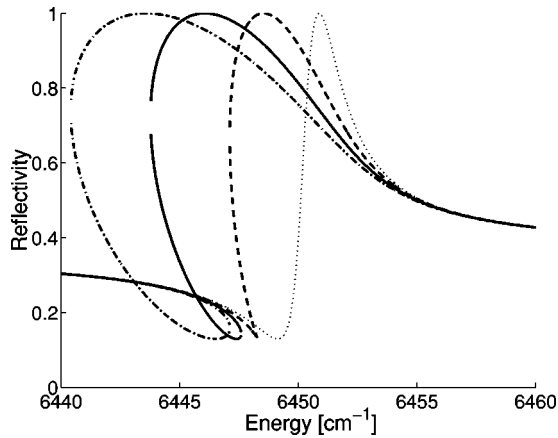
FIG. 5. Reflection spectra, in the presence of a downstream nonresonant scattering source R_{nr}, for an incident mode power of 2.2 mW (dotted), 44.0 mW (dashed), 87.6 mW (solid), and 131.6 mW (dash-dotted).

FIG. 6. Bistability of Fano reflectivity line shape at 6447.8 cm^{-1}. Arrows indicate the bistable loop that the system follows as the incident power is increased from zero and then decreased again. Circles (o), crosses (x), and asterisks (a) depict the three distinct solutions to the cubic equation found from Eq. (66). The "o," "x," and "a" labels introduced in this caption are for relating each solution to Fig. 10.

this is included, the corresponding hysteresis loops become smaller since the absorption reduces the peak reflectivity. Using a bulk two-photon absorption (TPA) coefficient for Al$_{0.18}$Ga$_{0.82}$As of 0.34 cm/GW [27], the hysteresis loop width is reduced by ≈ 14 mW (the curve of stars in Fig. 4). A theoretical prediction suggests that the TPA coefficient for Al$_{0.18}$Ga$_{0.82}$As should be 1.46 cm/GW [26]. When this is used the resulting hysteresis loop is given by the diamond curve in Fig. 4. We can conclude that as long as the TPA coefficient is not much larger than the latter value, TPA does not quench bistability in Al$_{0.18}$Ga$_{0.82}$As at this wavelength. However, TPA can significantly alter the hysteresis loop if it is greater than the former, experimentally observed value.

Now consider the impact of including a nonresonant downstream scattering source, with a reflectivity $R_{nr} = 0.6e^{-i\pi/2}$. Figure 5 shows the reflectivity spectra in this case for the same set of incident powers as in Fig. 3. As in the Lorentzian case, as the power is increased the change in the refractive index of the material shifts the resonant frequency to lower energy. However, the way in which the shifted resonance coherently adds to the stable nonresonant background results in drastically different line shapes than in the Lorentzian case. When bistability occurs it is possible for loops to appear in the spectra, and these loops result in drastically different hysteresis loops. The reflectivity, at 6447.8 cm^{-1}, as a function of incident power is shown in Fig. 6. This bistable loop is very different from that of the Lorentzian line shape. In this example the threshold power for the bistable loop has decreased significantly. The "on" switching occurs at 75 mW while the "off" switching occurs at only 32 mW. As is evident in Fig. 5, for high incident power the nonlinear reflectivity can be close to unity over a broad range of frequencies. This translates into distinct output power characteristics in the hysteresis loops. In this example, at high incident power, the reflected power becomes almost linear with the incident power (Fig. 6). Figure 7 illustrates the effect of TPA in this particular example of a nonresonant reflecting source. In this example the nonlinear absorption process significantly quenches the unity reflectivity
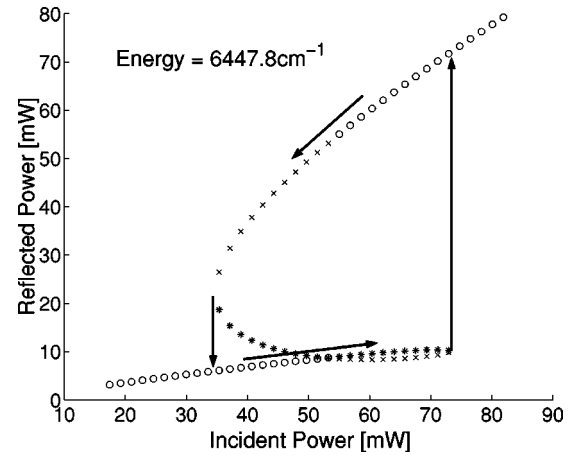
portion of the reflection spectra. The entire upper branch of the hysteresis loop is therefore significantly reduced in maximum power due to the absorption process.

It is therefore evident that it is important to include such nonresonant sources in any model of the nonlinear performance of coupled waveguides and cavities. On the other hand, nonresonant sources could be designed into the structure in order to engineer desired reflection spectra and hysteresis loops. The reflected field producing the Fano line shape is a result of interference between the sharp resonant field and the nonresonant background field that is slowly varying in both amplitude and phase. The nature of the Fano-like hysteresis curves depends strongly on the amplitude and phase of the downstream reflectivity, hence there is a rich
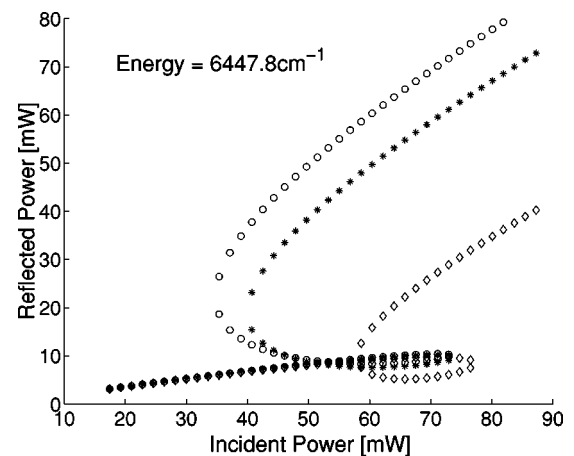

FIG. 7. Hysteresis loops showing effect of two-photon absorption for Fano resonances. The curve of circles is the result in the absence of TPA while the diamonds and asterisks are with a TPA coefficient of 1.46 cm/GW and 0.34 cm/GW, respectively. Energy is 6447.8 cm^{-1}.
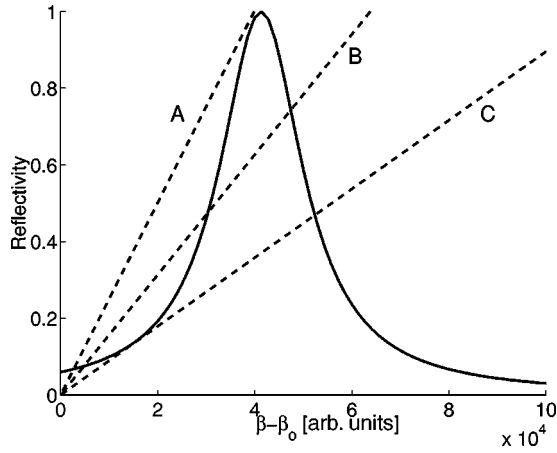
FIG. 8. Graphical solution for the Lorentzian line shape. Solid curve is independent of power and at a constant energy of 6447.8 cm^{-1} [Eq. (67)] and the dashed curves are independent of frequency and at a constant incident power [Eq. (68)] of 55 mW (curve A), 87.6 mW (curve B), and 153.6 mW (curve C).

diversity of behaviors that can be generated. We intend to address this point in subsequent publications.

We now turn to a stability analysis of the solutions involving nonzero downstream reflections in order to verify the hysteresis loop that the system will follow.

B. Stability analysis

The bistable response of 1D Fabry-Perot cavities is often discussed in terms of a graphical solution that clearly reveals the three allowed solutions in the multivalued reflectivity regime, as well as the stability of these solutions. Below we generalize to the Fano-line-shape case, the graphical approach used in Refs. [22,28] to analyze the stability of the solutions in the Lorentzian limit.

Defining a control parameter $\beta = \beta_o + \beta_2'|a_l|^2$, the expression for the reflectivity in the Lorentzian case becomes

$$R = \frac{i\widetilde{\omega}\Gamma}{\beta - i\widetilde{\omega}\Gamma},\tag{67}$$

and therefore $\beta_o = \widetilde{\omega}_l^2 - \widetilde{\omega}^2$ is the detuning from resonance in the linear limit, and β_2' is a factor representing the Kerr effect. Plotting $|R|^2$ as a function of $\beta - \beta_o$, one obtains the solid curve in Fig. 8. Since $\beta - \beta_o$ is proportional to $|a_l|^2$, the x axis can be taken to be $|a_l|^2$ in arbitrary units. This curve illustrates that, for some initial detuning from resonance, as $|a_l|^2$ is increased the system is pulled into resonance, as described above.

Using expression (63) for a_l to eliminate the resonant frequency dependence from the reflectivity, we arrive at the following independent relationship between R and the incident power:

$$R = R_{nr} + \frac{i\Gamma(1 + R_{nr})}{4\pi\widetilde{\omega}_l\chi_{l,w}^{0D}}\frac{a_l}{a_h}.\tag{68}$$

In the Lorentzian limit $R_{nr} = 0$, this can be used to obtain the following power-dependent relationship between β and R:

$$|R|^2 = \frac{\beta - \beta_o}{\beta_2|a_h|^2},\tag{69}$$

where $\beta_2 = (-4\pi\widetilde{\omega}_l^2\alpha/V_{mode})|4\pi\widetilde{\omega}_l\chi_{l,w}^{0D}/\Gamma|^2 = \beta_2'|4\pi\widetilde{\omega}_l\chi_{l,w}^{0D}/\Gamma|^2$. For each value of $|a_h|^2$, Eq. (69) defines a linear relationship between $|R|^2$ and $\beta - \beta_o$, where the slope depends on the incident power. The lines for $|a_h|^2$ corresponding to 55, 87.6, and 153.6 mW are plotted as dashed lines in Fig. 8. The intersection of these lines with the curve are the allowed solutions to the problem.

The stability of the solution can be found from the following considerations [22]. For the passive optical system considered here, the rate of change of the control parameter β is proportional to the difference between its driving function and its steady state value. Therefore, β satisfies the following dynamical equation:

$$\tau\frac{d\beta}{dt} = \beta_2'|a_l|^2 - \beta + \beta_o,\tag{70}$$

where τ is the cavity response time. Perturbing β from its steady state value by $\beta = \bar{\beta} + \delta\beta(t)$, one arrives at the following equation for $\delta\beta(t)$:

$$\tau\frac{d\delta\beta(t)}{dt} + \left(1 - \beta_2|a_h|^2\frac{d|R|^2}{d\beta}\right)\delta\beta(t) = 0,\tag{71}$$

which has solutions $\delta\beta(t) = \exp[-(\gamma/\tau)t]$, where γ is the expression in the parentheses of Eq. (71). For $|R|^2/\beta - \beta_o < d|R|^2/d(\beta - \beta_o)$ it is easy to see that γ is less than 0. Therefore the solutions to $\delta\beta(t)$ grow exponentially and thus these solutions are unstable. For $|R|^2/\beta - \beta_o > d|R|^2/d(\beta - \beta_o)$ the solutions are stable. This analysis indicates that the negative slope branch in the hysteresis loop of Fig. 4 is unstable. Let us now turn to the analysis of the Fano line shape.

When there is a nonzero downstream reflection, Eq. (67) easily generalizes to

$$R = R_{nr} + \frac{i\widetilde{\omega}\Gamma(1 + R_{nr})^2}{\beta - i\widetilde{\omega}\Gamma(1 + R_{nr})},\tag{72}$$

but Eq. (69) does not generalize. This is because the nonresonant contribution introduces a phase shift between the reflected field and the field in the cavity. This can be seen from Eq. (68), from which it is clear that $|R|^2$ is not directly proportional to $|a_l|^2$ in the Fano case. Therefore, the graphical solution cannot be expressed in a two-dimensional plot of $|R|^2$ versus $|a_l|^2$, because such a plot lacks any information about the phase of the two field components.

The graphical solution in this more general situation requires a four-dimensional plot of the real and imaginary parts of R as a function of real and imaginary a_l. We have verified that the three mutual intersections of the four surfaces (real and imaginary R at constant frequency (independent of
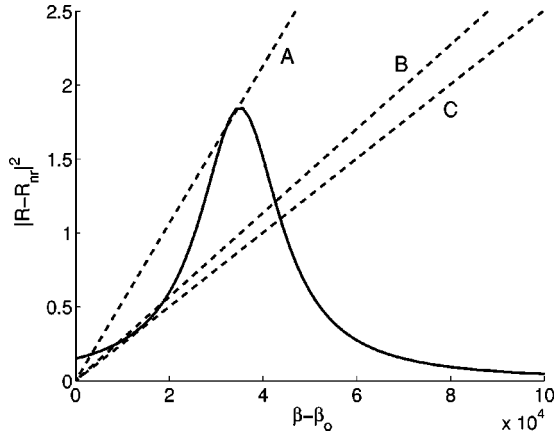
FIG. 9. Graphical solution for the Fano line shape. Solid curve is independent of power and at a constant energy of 6447.8 cm^{-1} and the dashed curves are independent of frequency and at a constant incident power [Eq. (73)] of 35 mW (curve A), 66.3 mW (curve B), and 74.7 mW (curve C).

FIG. 10. Plot of $|R-R_{nr}|^2$ as a function of energy for an incident power of 66.3 mW. The arrows point to the three distinct sections of the curve that originate from the three distinct solutions to the cubic equation derived from Eq. (66). The dashed is labeled "o" corresponding to the solutions depicted by circles in Fig. 6. The solid and dash-dot are, respectively, labeled x and a, and correspond to the crosses and asterisks in Fig. 6. The solid vertical line is a slice at 6447.8 cm^{-1} and illustrates that these numerical solutions are the same as the graphical ones found from curve B in Fig. 9.

power), and constant power (independent of frequency) indeed yield a graphical solution of the nonlinear reflectivity problem. However, the stability arguments for the Fano case would have to be generalized from a comparison of slopes in the graphical solution to the comparison of two-dimensional gradients. Instead of proceeding in this fashion we introduce a simpler stability argument that is essentially the same as in the Lorentzian limit.

If one uses $|R-R_{nr}|^2$ instead of $|R|^2$ in Eq. (68), then there is a power-dependent proportionality to $\beta-\beta_o$, namely,

$$|R-R_{nr}|^2 = \frac{\beta-\beta_o}{\beta_2^{nr}|a_h|^2}, \quad (73)$$

where $\beta_2^{nr} = \beta_2'|4\pi\widetilde{\omega}_l\chi_{l,w}^{0D}/\Gamma(1+R_{nr})|^2$. A power-independent relationship for the function $|R-R_{nr}|^2$ is obtained directly from Eq. (72). Plotting the latter curve at 6447.8 cm^{-1} and the former at incident powers of 35, 66.3, and 74.7 mW, we arrive at the graph shown in Fig. 9. In contrast to the Lorentzian case, this diagram does *not* represent a full graphical solution for the reflectivity since one cannot extract the reflectivity from a knowledge of $|R-R_{nr}|^2$. However, this is a graphical solution to $|R-R_{nr}|^2$. Upon solving the full cubic equation for an incident power of 66.3 mW and plotting $|R-R_{nr}|^2$ rather than $|R|^2$, we produce Fig. 10. The solutions shown in this figure correspond exactly to the crossing points of Fig. 9. The solid vertical line at an energy of 6447.8 cm^{-1} illustrates this equivalence. Therefore each of the three solutions found graphically in Fig. 9 can be directly associated with one of the three distinct solutions to the cubic equation derived from Eq. (66). The three distinct values of $|R-R_{nr}|^2$ arising from the three distinct analytic solutions to the cubic equation are labeled as "o," "x," and "a" in Fig. 10. The o, x, and a solutions correspond to the circle, cross, and asterisk solutions for the reflected power that results from the same three solutions to the cubic equation. There is therefore a clear link between
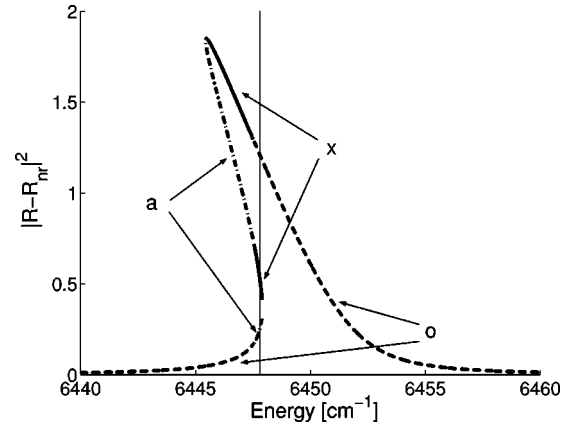
the graphical solutions in Fig. 9 and the numerical hysteresis loop in Fig. 6. This is possible since R_{nr} is single valued. A stability argument of the three graphical solutions in Fig. 9 can then be used to investigate the stability of the three branches in the hysteresis loop.

Assuming the same feedback relaxation equation given in Eq. (70), the equation for $\delta\beta(t)$ in the Fano case becomes

$$\tau\frac{d\,\delta\beta(t)}{dt} + \left(1-\beta_2^{nr}|a_h|^2\frac{d|R-R_{nr}|^2}{d\beta}\right)\delta\beta(t)=0, \quad (74)$$

which again has the solutions $\delta\beta(t)=\exp[-(\gamma^{nr}/\tau)t]$. It follows that solutions in the region for which $|R-R_{nr}|^2/\beta -\beta_o < d|R-R_{nr}|^2/d(\beta-\beta_o)$ are unstable while solutions when the opposite is true are stable. Since these unstable solutions correspond to the internal branch of the Fano-derived hysteresis loop in Fig. 6 we conclude that this internal branch is unstable and thus the loop follows the path depicted by the arrows in Fig. 6. We feel that our approach greatly simplifies earlier stability arguments for hysteresis loops associated with Fano resonances, approaches that relied on absorption within the nonlinear material [29], or phenomenological parameters [30].

Finally, one of the most striking features of these Fano-derived hysteresis loops is the fact that different branches of the curve can cross each other. These crossing points in plots of output power versus input power do not correspond to degenerate solutions. This is because each solution still has a unique phase with respect to the incident field. It is not enough that the amplitude of the electric field (proportional to power) for each solution is the same, but their phases must also be equal to render the solutions degenerate. These crossing points therefore represent no critical switching point for the system. In fact, the stability analysis above indicates that one of the two solutions is unstable and therefore there is

only one allowed solution at these crossing points. Nevertheless, as is evident from the example presented here, bistable loops resulting from Fano resonances can have significantly different properties than the usual Lorentzian-derived loops.

V. CONCLUSIONS

In this paper we derived a simple analytic solution for the reflection of a guided mode that interacts with a Kerr-active nonlinear resonant cavity and a downstream nonresonant scattering source. A second-order wave equation for the electric field is solved using an intuitive expansion of the associated Green's function and the field, rather than solving the equivalent first-order equations for both the electric and magnetic fields, as has been reported by others [3,6,5]. All of the relevant linear and nonlinear coupling mechanisms are clearly and explicitly associated with well-defined overlap integrals involving electric field Bloch states and dielectric perturbations. The approximations required to obtain this simple analytic solution are made clear. The simple form of the solution avoids the need for iterative solutions. Instead, an independent cubic equation for the localized mode amplitude is solved first, and the result is used to obtain the reflectivity for a given incident power.

For moderately high-Q ($Q \sim 4000$) resonant cavities with mode volumes of the order of 0.05 μm^3, which should be attainable using various PC fabrication technologies, the model predicts Kerr-related bistable behavior at incident power levels of ~ 40 mW in $Al_{0.18}Ga_{0.82}As$. Although two-photon absorption reduces the maximum range of the hysteresis loops, the reduction is estimated to be only a few percent.

The presence of nonresonant downstream scattering sources in the waveguide results in Fano-like resonant features in the reflection spectra. In the nonlinear regime the coherent superposition of the stable background and power-dependent resonant contribution result in topologically distinct hysteresis loops (in contrast to the more common Lorentzian situation). We generalized conventional stability arguments in order to determine which branches of these hysteresis loops are stable.

From this work we conclude that photonic crystals made from $Al_{0.18}Ga_{0.82}As$ offer the potential for realizing bistable optical functionality at power levels of the order of 40 mW, without significant impairment due to two-photon absorption. It is also clear that nonresonant, downstream reflections can significantly modify the nature of the bistable reflectivity. This fact may be used to obtain more flexibility in designing nonlinear devices, but regardless, it shows that these reflections should not be overlooked in analyzing the nonlinear behavior of waveguides that interact with resonant localized cavities.

APPENDIX: ORTHOGONALITY OF BASIS

In this appendix we discuss how the orthogonality relation of Eq. (20) is intuitively justified within the weak coupling limit.

First, if n and m correspond to guided mode eigenstates, then Eq. (20) can be written as $\langle \vec{\phi}_{k_i} | \hat{\epsilon}_w | \vec{\phi}_{k_j} \rangle + 4\pi \langle \vec{\phi}_{k_i} | \hat{\chi}^{0D} | \vec{\phi}_{k_j} \rangle = \delta_{k_i, k_j}$. Since the first term on the left-hand side of this expression is the rigorous orthogonality of the guided mode eigenstates, it follows that $\langle \vec{\phi}_{k_i} | \hat{\chi}^{0D} | \vec{\phi}_{k_j} \rangle = 0$. The overlap integral $\langle \vec{\phi}_{k_i} | \hat{\chi}^{0D} | \vec{\phi}_{k_j} \rangle$ describes the direct renormalization of a single guided eigenstate (if $n = m = k_i$), or the direct coupling between two guided eigenstates (if $n = k_i$ and $m = k_j$), by the presence of the cavity. In the weak coupling regime this will be negligible and it is therefore valid to neglect it. An analogous argument involving the localized state results in $\langle \vec{\phi}_l | \hat{\chi}^{1D} | \vec{\phi}_l \rangle = 0$, which is also valid within our weak coupling limit.

If either n or m corresponds to a guided mode eigenstate and the other to the localized mode, then there are two equally acceptable ways to expand Eq. (20): $\langle \vec{\phi}_{k_i} | \hat{\epsilon}_w | \vec{\phi}_l \rangle + 4\pi \langle \vec{\phi}_{k_i} | \hat{\chi}^{0D} | \vec{\phi}_l \rangle = 0$ and $\langle \vec{\phi}_{k_i} | \hat{\epsilon}_d | \vec{\phi}_l \rangle + 4\pi \langle \vec{\phi}_{k_i} | \hat{\chi}^{1D} | \vec{\phi}_l \rangle = 0$. Multiplying each by the appropriate factor of $\tilde{\omega}^2$ and subtracting, one obtains $\tilde{\omega}_{k_i}^2 \langle \vec{\phi}_{k_i} | \hat{\chi}^{0D} | \vec{\phi}_l \rangle - \tilde{\omega}_l^2 \langle \vec{\phi}_{k_i} | \hat{\chi}^{1D} | \vec{\phi}_l \rangle = 0$, where the unitarity condition has been used to eliminate the factors containing ϵ. Therefore, the assumption of $\langle \vec{\phi}_{k_i} | \hat{\epsilon}_t | \vec{\phi}_l \rangle = 0$ in a physical system requires that $\tilde{\omega}_{k_i}^2 \langle \vec{\phi}_{k_i} | \hat{\chi}_{0D} | \vec{\phi}_l \rangle - \tilde{\omega}_l^2 \langle \vec{\phi}_{k_i} | \hat{\chi}^{1D} | \vec{\phi}_l \rangle = 0$. While this constraint is not quite as simple as the ones above, it is still very useful.

Consider the unitarity condition of Eq. (19). Using the definition of both $\hat{\epsilon}_w$ and $\hat{\epsilon}_d$ and some simple algebra it is possible to derive the following expression:

$$\frac{(\tilde{\omega}_{k_i}^2 - \tilde{\omega}_l^2)}{4\pi} \langle \vec{\phi}_{k_i} | \hat{\epsilon}_t | \vec{\phi}_l \rangle = \tilde{\omega}_{k_i}^2 \langle \vec{\phi}_{k_i} | \hat{\chi}^{0D} | \vec{\phi}_l \rangle - \tilde{\omega}_l^2 \langle \vec{\phi}_{k_i} | \hat{\chi}^{1D} | \vec{\phi}_l \rangle. \quad (A1)$$

Due to the regularity of the function $\langle \vec{\phi}_{k_i} | \hat{\epsilon}_t | \vec{\phi}_l \rangle$, it follows from the above that on resonance $\tilde{\omega}_{k_i}^2 \langle \vec{\phi}_{k_i} | \hat{\chi}^{0D} | \vec{\phi}_l \rangle - \tilde{\omega}_l^2 \langle \vec{\phi}_{k_i} | \hat{\chi}^{1D} | \vec{\phi}_l \rangle = 0$. This on-resonant result, which is independent of the value of the function $\langle \vec{\phi}_{k_i} | \hat{\epsilon}_t | \vec{\phi}_l \rangle$, is simply a consequence of unitarity. In the weak coupling regime we are only concerned with the response of the system near resonance, since the resonance is relatively narrow in frequency. The smooth continuous nature of the function $\langle \vec{\phi}_{k_i} | \hat{\epsilon}_t | \vec{\phi}_l \rangle$ verifies that $\tilde{\omega}_{k_i}^2 \langle \vec{\phi}_{k_i} | \hat{\chi}^{0D} | \vec{\phi}_l \rangle - \tilde{\omega}_l^2 \langle \vec{\phi}_{k_i} | \hat{\chi}^{1D} | \vec{\phi}_l \rangle$ is sufficiently small near resonance. This simply expresses that near resonance the response of the structure is dominated by guided-localized mode coupling, while away from resonance this coupling mechanism becomes of the order of the weak mode renormalization process, and thus we cannot neglect one with respect to the other.

We can therefore conclude that our orthogonality condition given in Eq. (20) is a valid approximation within the weak coupling limit. Intuitively, it corresponds to neglecting the direct renormalization of the guided and localized mode with respect to the dominate localized-guided mode coupling process.

Furthermore, for a particular waveguide-resonator structure the deviation of the functions $\langle \vec{\phi}_{k_j} | \hat{\chi}^{0D} | \vec{\phi}_{k_i} \rangle$, $\langle \vec{\phi}_l | \hat{\chi}^{1D} | \vec{\phi}_l \rangle$, and $\tilde{\omega}_{k_i}^2 \langle \vec{\phi}_{k_i} | \hat{\chi}^{0D} | \vec{\phi}_l \rangle - \tilde{\omega}_l^2 \langle \vec{\phi}_{k_i} | \hat{\chi}^{1D} | \vec{\phi}_l \rangle$ from zero represents a measure of the validity of our solution for that structure. If the deviation from zero of these functions is much smaller than the value of the dominant coupling mechanism quantified by $\langle \vec{\phi}_l | \hat{\chi}^{0D} | \vec{\phi}_{k_i} \rangle$, then one can conclude that the system lies within our weak coupling limit. Note, the first two functions, being directly dependent on the spatial separation of the guide and cavity, represent a spatial constraint, while the final expression corresponds to a constraint in frequency detuning.

[1] J. D. Joannopoulos, R. D. Meade, and J. N. Winn, *Photonic Crystals: Molding the Flow of Light* (Princeton University Press, Princeton, NJ 1995).

[2] K. Sakoda, *Optical Properties of Photonic Crystals* (Springer, Berlin, 2001).

[3] Y. Xu, Y. Li, R.K. Lee, and A. Yariv, Phys. Rev. E **62**, 7389 (2000).

[4] S. Fan, P.R. Villeneuve, J.D. Joannopoulos, and H.A. Haus, Phys. Rev. Lett. **80**, 960 (1998).

[5] S. Fan, P.R. Villeneuve, J.D. Joannopoulos, M.J. Khan, C. Manolatou, and H.A. Haus, Phys. Rev. B **59**, 15 882 (1999).

[6] S. Fan, P.R. Villeneuve, J.D. Joannopoulos, and H.A. Haus, Phys. Rev. B **64**, 245302 (2001).

[7] C. Manolatou, M.J. Khan, S. Fan, P.R. Villeneuve, H.A. Haus, and J.D. Joannopoulos, Int. J. Quantum Chem. **35**, 1322 (1999).

[8] J. Moosburger, M. Kamp, A. Forchel, U. Oesterle, and R. Houdre, J. Appl. Phys. **91**, 4791 (2002).

[9] S. Noda, A. Chutinan, and M. Imada, Nature (London) **407**, 608 (2000).

[10] S. Nishikawa, S. Lan, N. Ikeda, Y. Sugimoto, H. Ishikawa, and K. Asakawa, Opt. Lett. **27**, 2079 (2002).

[11] M. Notomi, K. Yamada, A. Shinya, J. Takahashi, C. Takahashi, and I. Yokohama, Phys. Rev. Lett. **87**, 253902 (2001).

[12] H. Kosaka, T. Kawashima, A. Tomita, M. Notomi, T. Tamamura, T. Sato, and S. Kawakami, Phys. Rev. B **58**, R10096 (1998).

[13] K. Sakoda and K. Ohtaka, Phys. Rev. B **54**, 5742 (1996).

[14] For a review of some of this work, see J. Opt. Soc. Am. B, **19** (9) (2002), special issue on nonlinear photonic crystals, edited by Charles M. Bowden and Aleksei M. Zheltiko.

[15] A. Hache and M. Bourgeois, Appl. Phys. Lett. **77**, 4089 (2000).

[16] D. Pezzetta, C. Sibilia, M. Bertolotti, R. Ramponi, R. Osellame, M. Marangoni, J.W. Haus, M. Scalora, M.J. Bloemer, and C.M. Bowden, J. Opt. Soc. Am. B **19**, 2102 (2002).

[17] T.V. Dolgova, A.I. Maidykovski, M. Martemyanov, A.A. Fedyanin, O.A. Aktsipetrov, G. Marowsky, V.A. Yakovlev, and G. Mattei, Appl. Phys. Lett. **81**, 2725 (2002).

[18] M. Banaee, A.R. Cowan, W. Jiang, C. Kaiser, X. Shen, and Jeff F. Young, PECS-IV: Nonlinear Response of Microcavity States in 2D Planar Waveguide-Based Photonic Crystals 2002, edited by Shawn-Yu Lin (unpublished).

[19] Y. Dumeige, I. Sagnes, P. Monnier, P. Vidakovic, I. Abram, C. Meriadec, and A. Levenson, Phys. Rev. Lett. **89**, 043901 (2002).

[20] A.R. Cowan and J.F. Young, Phys. Rev. B **65**, 085106 (2002).

[21] M.G. Banaee, A.R. Cowan, and J.F. Young, J. Opt. Soc. Am. B **19**, 2224 (2002).

[22] H. M. Gibbs, *Optical Bistability: Controlling Light with Light* (Academic Press, New York, 1985).

[23] J.C. Knight, G. Cheung, F. Jacques, and T.A. Birks, Opt. Lett. **22**, 1129 (1997).

[24] Marin Soljacic, Mihai Ibanescu, Steven G. Johnson, Yoel Fink, and J.D. Joannopoulous, Phys. Rev. E **66**, 055601(R) (2002).

[25] Shanhui Fan, Appl. Phys. Lett. **80**, 908 (2002).

[26] D. Hutchings and B. Wherrett, Phys. Rev. B **50**, 4622 (1994).

[27] A. Villeneuve, C.C. Yang, G.I. Stegeman, C.-H. Lin, and H.-H. Lin, Appl. Phys. Lett. **62**, 2465 (1993).

[28] J. A. Goldstone, *Laser Handbook* (North-Holland, Amsterdan, 1985), Vol. 4.

[29] P. Vincent, N. Paraire, M. Neviere, A. Koster, and R. Reinisch, J. Opt. Soc. Am. B **2**, 1106 (1985).

[30] M. Neviere, E. Popov, and R. Reinisch, J. Opt. Soc. Am. A **12**, 513 (1995).